Eur Biophys J (1995) 23: 385–398

European Biophysics Journal

Low temperature optical absorption spectroscopy: an approach to the study of stereodynamic properties of hemeproteins

Antonio Cupane, Maurizio Leone, Eugenio Vitrano, Lorenzo Cordone

Istituto di Fisica dell'Università and GNSM-INFM, Via Archirafi 36, I-90123 Palermo, Italy (Fax: +39-91-6162461)

Received: 6 May 1994 / Accepted in revised form: 3 October 1994

Abstract. In this short review we show how suitable analysis of the temperature dependence of the optical absorption spectra of metalloproteins can give insight into their stereodynamic properties in the region of the chromophore. To this end, the theory of coupling between an intense allowed electronic transition of a chromophore and Franck-Condon active vibrations of the nearby atoms is applied to the Soret band of hemeproteins to obtain an analytical expression suitable for fitting the spectral profile at various temperatures. The reported approach enables one to separate the various contributions to the overall bandwidth together with the parameters that characterize the vibrational coupling. The thermal behavior of these quantities gives information on the dynamic properties of the active site and on their dependence upon protein structure and ligation state. The Soret band of hemeproteins appears to be coupled to high frequency vibrational modes of the heme group (as already shown by resonance Raman spectroscopy) and to a "bath" of low frequency modes most likely deriving from the bulk of the protein. For the deoxy derivatives inhomogeneous broadening arising from conformational heterogeneity appears to contribute substantially to the linewidth. The data indicate the onset, at temperatures near 180 K, of large scale anharmonic motions that can be attributed to jumping among different conformational substates of the protein.

Key words: Protein dynamics – Vibrational coupling – Anharmonic motions – Conformational substates

Introduction

It is well known that the optical absorption spectra of metalloproteins depend markedly on temperature (Knowles et al. 1975; San Biagio et al. 1977; Dooley et al. 1979; Solomon et al. 1980; Browett and Stillman 1984; Allendorf et al. 1985; Cordone et al. 1986; Leone et al. 1987; Di Iorio et al. 1991; Vitrano et al. 1993); as an example we shown in Fig. 1 the Soret band of Asian elephant MbCO at various temperatures in the range 300-20 K. Three main effects are observed on lowering the temperature: i) halfwidth narrowing, ii) peak frequency shift, iii) integrated intensity variations.

The physical origin of the marked changes in the absorption profile can be traced to the coupling of the electronic transition responsible for the absorption band with the thermal motions of the nearby atoms (Huang and Rhys 1950; Markham 1959; Pryce 1966). For this reason, accurate optical absorption measurements performed from room temperature to 10 K, together with a suitable theoretical analysis of electron-vibrations interactions, can give relevant information on the dynamic properties of the protein in the region of the chromophore.

This approach has been exploited by our group in recent years (Di Pace et al. 1992; Cupane et al. 1993 a, b) and is briefly reviewed in this paper. In the "Theoretical Section" we describe the basic theory of the linear coupling between an intense isolated electronic transition and the vibrations of the nearby matrix. The aim of this section is to obtain an analytical expression suitable for fitting the optical absorption spectra in the entire temperature interval. Extension of the theory to include electron-vibrations quadratic coupling is given in Appendix A. In the section "Some Experimental Results" the theory is applied to analyze the temperature dependence of the Soret band lineshape in liganded and unliganded sperm whale myoglobin to obtain information on the dynamic properties of the system. Limitations of the described approach are also discussed at the end of the "Theoretical Section" and the simplified "Method of Moments" is outlined in Appendix B.

Abbreviations: MbCO, Carbonmonoxy-myoglobin; Mb, Deoxy-myoglobin; Mb^{3+}, Aquomet-myoglobin; SWMbCO, Spermwhale carbonmonoxy-myoglobin; SWMb, Spermwhale deoxy-myoglobin

Correspondence to: A. Cupane

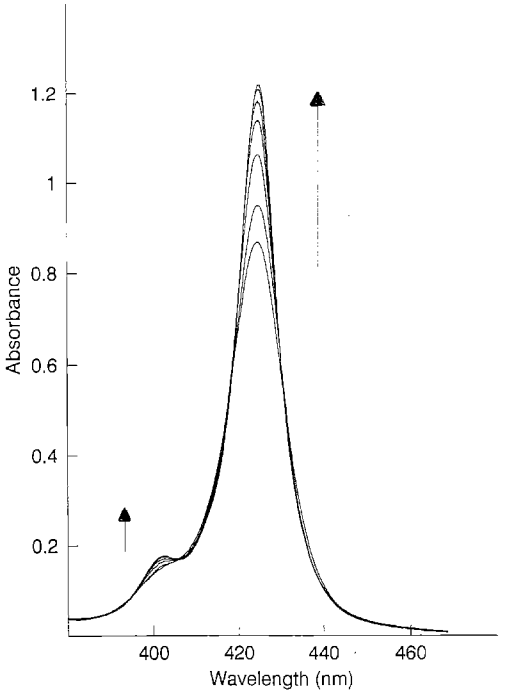

Fig. 1. Optical absorption spectra (Soret band) of Asian elephant MbCO in the temperature range 20–300 K. The arrows indicate the directions of spectral changes observed on lowering the temperature. Experimental conditions are: $\approx 4\times10^{-6}$ M protein concentration; 0.1 M phosphate buffer pH 7 (measured in water at room temperature); 65% v/v glycerol/water. Note the high quality of the spectra, that is due to the absence of sample cracking in the whole temperature range

Theoretical section

The probability per unit time for an isolated electronic system to be promoted by an electromagnetic field from a ground state a (with energy value E_a and eigenfunction Ψ_a) to an excited state b (with energy value E_b and eigenfunction Ψ_b) is given by (Bransden and Joachain 1983):

$$W_{ba} = \frac{16\pi^4}{3h^2}\frac{1}{4\pi\varepsilon_0}\left|R_{ba}\right|^2 \rho(\nu)\,\delta(\nu-\nu_{ba}) \qquad (1)$$

where $R_{ba}=\langle\Psi_b/er/\Psi_a\rangle$ is the quantum-mechanical matrix element of the electric dipole moment (transition moment), $\rho(\nu)$ is the energy density of the electromagnetic field, $\nu_{ba}=(E_b-E_a)/h$ is the frequency value matching the quantum jump (see Fig. 2a) and h is the Planck's constant.

At each promotional event the field energy changes by $h\nu_{ba}$, therefore for a dl path length of a sample having n_0 identical non-interacting absorbers per unit volume in the ground state, the differential energy loss is[1]:

$$-dI(\nu) = I(\nu)\,n_0\frac{16\pi^4}{3h^2}\frac{1}{4\pi\varepsilon_0}\frac{h\nu}{c} \cdot\delta\left(\nu-\frac{E_b-E_a}{h}\right)\left|R_{ba}\right|^2 dl \qquad (2)$$

where $I(\nu)$ is the energy flowing in 1 s through a unit cross-section area and is related to the energy density by $I(\nu)=c\,\rho(\nu)$. By integration over a 1 cm path of absorbing material, one obtains the following expression for the absorbance as a function of ν:

$$F(\nu) = Ln\frac{I_0(\nu)}{I(\nu)} = n_0\frac{4\pi^3}{3h\varepsilon_0 c}\left|R_{ba}\right|^2\nu\,\delta\left[\nu-\frac{(E_b-E_a)}{h}\right]. \qquad (3)$$

Owing to the finite lifetime (τ) of the excited state, the δ function in Eq. (3) can be replaced by a Lorentzian shape function (with $2\,\Gamma=1/\tau$), i.e.:

$$F(\nu) = n_0\frac{4\pi^2}{3h\varepsilon_0 c}\left|R_{ba}\right|^2\nu\frac{\Gamma}{[\nu-(E_b-E_a)/h]^2+\Gamma^2} \qquad (4)$$

If the absorbers are embedded in a matrix, coupling of the electronic transition to vibrational modes of the surrounding nuclei can affect both the energy difference (E_b-E_a) and the transition moment R_{ba}.

Let us consider N vibrational modes of the matrix; the total energy for the ground state can be written, within the Born-Oppenheimer and adiabatic approximations, as:

$$E_a = \eta_a + \frac{1}{2}h^2\sum_{j=1}^{N}\nu_j^2(a)\,q_j^2 \qquad (5)$$

where the normal nuclear coordinates q_j[2] describe the nuclear vibrations coupled to the ground electronic state (set q), $\nu_j(a)$ are the relative frequencies and η_a is the energy of the electronic ground state when all the nuclei are at rest in their equilibrium positions $q=0$. For the excited state, we can write:

$$E_b = E_a + \Delta E(q) = E_a + \Delta E_0 + \sum_j\alpha_j q_j + \frac{1}{2}\sum_j\alpha_{jj}\,q_j^2 \qquad (6)$$

where

$$\Delta E_0 = \Delta E_{q=0};\quad \alpha_j = \left.\frac{\partial\Delta E}{\partial q_j}\right|_{q=0};\quad \alpha_{jj} = \left.\frac{\partial^2\Delta E}{\partial q_j^2}\right|_{q=0}$$

In (6) we have expanded the total energy difference between the excited and ground states in terms of the coordinates q_j up to second order and we have neglected mixing between normal modes (i.e. $\alpha_{jk}=|\partial^2(\Delta E)/\partial q_j\,\partial q_k|_{q=0}=0$).

Inserting (5) into (6) and making use of the transformation $Q_j=q_j-\Delta_j=q_j+\alpha_j/[h^2\,\nu_j^2(b)]$, with $\nu_j^2(b)-\nu_j^2(a)=\alpha_{jj}/h^2$, one obtains:

$$E_b = \eta_b + \frac{1}{2}h^2\sum_{j=1}^{N}\nu_j^2(b)\,Q_j^2 \qquad (7)$$

[1] The process of stimulated emission is not considered in this treatment since we will deal only with the Soret band of hemeproteins, where the energy difference between the electronic states involved is $h\nu\simeq 4\cdot10^{-19}$ J, so that only the ground electronic state is populated at room temperature ($k_B T=4\cdot10^{-21}$ J at $T=300$ K)

[2] Note that the normal nuclear coordinate q_j is defined as: $q_j=X_j\mu_j^{1/2}/h$, where X_j is the real nuclear displacement and μ_j is the reduced mass associated with the j-th normal mode

where

$$\eta_b = \eta_a + \Delta E_0 - \frac{1}{2}\sum_j \frac{\alpha_j^2}{h^2 \nu_j^2(b)}$$
$$= \eta_a + \Delta E_0 - \frac{1}{2}\sum_j h^2 \nu_j^2(b) \Delta_j^2.$$

Equation (7) is formally identical to Eq (5). It is therefore seen that the electronic promotion from state a to state b has, in general, two effects on nuclear vibrations:

1) it makes the set of normal coordinates change from q_j to $Q_j = q_j - \Delta_j$ (i.e. it displaces the equilibrium position of the nuclei by a quantity Δ_j);
2) it makes the frequencies of normal modes change from $\nu_j(a)$ to $\nu_j(b)$, such that $\nu_j^2(b) - \nu_j^2(a) = \alpha_{jj}/h^2$.

The first effect is related to electron-vibrations linear coupling and the quantity $S_j = \frac{h}{2}\nu_j(b)\Delta_j^2$ is called the linear coupling constant; the second effect is related to electron-vibrations quadratic coupling and the quantity $R_j = \nu_j^2(b)/\nu_j^2(a)$ is called the quadratic coupling constant.

We will consider here an electronic transition having only linear coupling with the surrounding matrix (i.e. $\alpha_{jj} = 0$ and $\nu_j(b) = \nu_j(a) = \nu_j$); the case where both linear and quadratic coupling is present will be discussed in Appendix A.

Considering only linear coupling (5) and (7) become:

$$E_a = \eta_a + \frac{1}{2}h^2 \sum_{j=1}^{N} \nu_j^2 q_j^2 \qquad (5\text{bis})$$

$$E_b = \eta_b + \frac{1}{2}h^2 \sum_{j=1}^{N} \nu_j^2 Q_j^2 \qquad (7\text{bis})$$

and therefore:

$$\left.\frac{E_b - E_a}{h}\right|_{m,n} = \frac{\Delta E_0}{h} - \sum_{j=1}^{N} S_j \nu_j + \sum_{j=1}^{N}\left(m_j + \frac{1}{2}\right)\nu_j$$
$$- \sum_{j=1}^{N}\left(n_j + \frac{1}{2}\right)\nu_j = \nu_{00} + \sum_{j=1}^{N}(m_j - n_j)\nu_j \quad (8)$$

where $\nu_{00} = \Delta E_0/h - \sum_j S_j \nu_j$ and n_j and m_j are the vibrational quantum numbers characterizing the ground and excited electronic states respectively; moreover we note that (8) refers to the entire set of possible values of energy difference between ground and excited state, depending upon all possible values of the set $\{m_j, n_j\}$ of quantum numbers.

In order to obtain a suitable expression of the transition moment R_{ba}, we make use of the Born-Oppenheimer approximation and write the total eigenfunction as a product of an electronic eigenfunction (depending on both electronic coordinates ξ and vibrational coordinates q) and a vibrational eigenfunction (depending only on q):

$$\Psi(\xi, q) = \Phi(\xi, q)\ \Theta(q) \qquad (9)$$

As already mentioned, q stands for the set q_j of normal nuclear coodinates; this set q, like the eigenfunction $\Theta(q)$, is independent of the electronic coordinates although it is dependent upon the electronic state: for this reason, in the following $\Theta(q)$ and $\Theta(Q)$ will stand for the vibrational eigenfunctions when electrons are in the ground and excited state respectively.

By considering the electric dipole moment as composed by a part due to the electrons (M_e) and a part due to the nuclei (M_n), one has (Herzberg 1966):

$$R_{ba} = \int \Phi_b^*\, \Theta^*(Q)\, M_e\, \Theta(q)\, \Phi_a\, \mathrm{d}\tau$$
$$+ \int \Phi_b^*\, \Theta^*(Q)\, M_n\, \Theta(q)\, \Phi_a\, \mathrm{d}\tau. \qquad (10)$$

Since M_n depends only upon vibrational coordinates q, while M_e and Φ are assumed to depend upon the nuclear equilibrium positions $q = 0$ and not upon the vibrational coordinates q (Condon approximation), Eq. (10) can be readjusted as follows:

$$R_{ba} = \int \Phi_b^*|_{(\xi, q=0)}\, M_e|_{(\xi, q=0)}\, \Phi_a|_{(\xi. q=0)}\, \mathrm{d}\tau_e$$
$$\times \int \Theta^*(Q)\, \Theta(q)\, \mathrm{d}\tau_v$$
$$+ \int \Theta^*(Q)\, M_n(q)\, \Theta(q)\, \mathrm{d}\tau_v$$
$$\times \int \Phi_b^*|_{(\xi, q=0)}\, \Phi_a|_{(\xi, q=0)}\, \mathrm{d}\tau_e. \qquad (11)$$

Owing to the orthogonality of electronic eigenfunctions the second term vanishes; within the above approximations the transition moment R_{ba} is therefore given by:

$$R_{ba} = R_e \times \int \Theta^*(Q)\, \Theta(q)\, \mathrm{d}\tau_v \qquad (12)$$

where we have indicated with the symbol R_e the quantity $\int \Phi_b^*|_{(\xi, q=0)}\, M_e\, \Phi_a|_{(\xi, q=0)}$. Making use of (8) and (12), (4) becomes:

$$F(\nu) = M\nu \sum_{\{m_j, n_j\}} \left| \int_{-\infty}^{\infty} \Theta^*(Q)\, \Theta(q)\, \mathrm{d}\tau_v \right|^2$$
$$\cdot P(n, T)\, \frac{\Gamma}{\left[\nu - \nu_{00} - \sum_j (m_j - n_j)\nu_j\right]^2 + \Gamma^2} \qquad (13)$$

where $M = n_0 \frac{4\pi^2}{3h\varepsilon_0 c} R_e^2$, and $P(n, T)$ is the probability of finding, at a given temperature T, the absorbing centers in the ground electronic state and in the vibrational state characterized by the set of quantum number n[3].

Concerning the term $\left| \int_{-\infty}^{\infty} \Theta^*(Q)\, \Theta(q)\, \mathrm{d}\tau_v \right|^2$, we note that if there is no coupling between the electronic transition and the vibrational modes, no readjustment takes place in the nuclear coordinates following the electronic promotion (see Fig. 2a), and therefore the set Q coincides with q and, owing to the orthogonality of harmonic oscillator wavefunctions, only terms with $m_j = n_j$ contribute to the absorption. In the presence of coupling (see Fig. 2b) $Q \neq q$

[3] A more general treatment could consider the dependence of M_e upon nuclear coordinates q. Expansion of M_e in series of q_j gives:

$$M_e = M_e|_{(\xi, q=0)} + \sum_j \left.\frac{\partial M_e}{\partial q_j}\right|_{(\xi, q=0)} q_j + \ldots$$

For an allowed transition, such as the one that gives rise to the Soret band of hemeproteins, the zeroth order term of the above expansion dominates and the other terms can be neglected: this is the

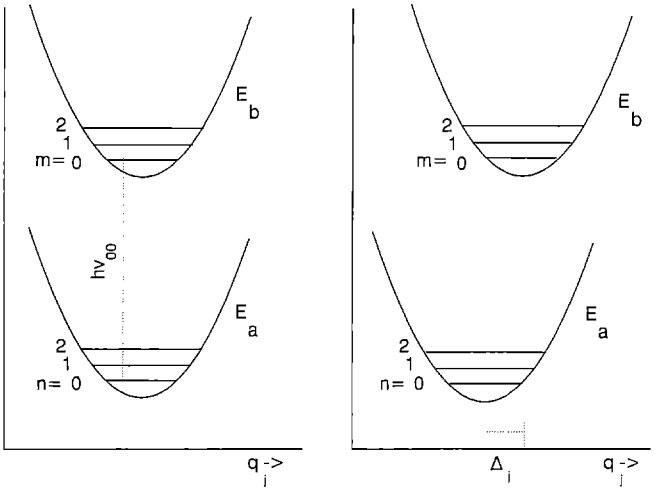

Fig. 2. Configuration coordinate diagram. $E(a)$ and $E(b)$ are the potential energy curves for the ground and excited electronic states respectively; q_j represents a generalized nuclear coordinate. Electronic transitions occur instantaneously with respect to the timescale of nuclear motions (*vertical arrows*)

and also terms with $m_j \neq n_j$ will contribute to the absorption: such contributions will have relative intensity weighted by the Boltzmann factor $P(n,T)$ and will occur at frequency $\nu = \nu_{00} + \sum_j (m_j - n_j)\nu_j$ (see (8)).

Since we have considered N vibrational modes, the total vibrational eigenfunctions for the ground and excited electronic state are:

$$\Theta(q) = \prod_{j=1}^{N} \theta_j(q_j); \quad \Theta(Q) = \prod_{j=1}^{N} \theta_j(q_j - \Delta_j) \tag{14}$$

where θ_j is the generic eigenstate of a harmonic oscillator with frequency ν_j.

approximation used in this paper. As a consequence, no variation of the transition moment (and therefore of the integrated intensity) by lowering the temperature is expected in the Soret band, and indeed only a few percent increase, compatible with the thermal contraction of the sample, is observed (Cordone et al. 1986; Cupane et al. 1988).

For less intense bands, such as the Q bands or the charge transfer bands in the absorption spectra of hemeproteins, the first order terms in the above M_e expression cannot be neglected; this further complicates the theory since it introduces non-Condon electron-vibrations couplings whose treatment is beyond the scope of this paper. For totally forbidden transitions, the term $M_e|_{(\xi, q=0)}$ does not contribute to the transition moment which is therefore entirely due to non-Condon vibronic coupling. For such bands, increase, decrease or even no variation of integrated intensity can be observed by lowering the temperature, depending on the particular band investigated. The analysis of the temperature dependence of integrated intensity can be particularly interesting in the case of charge transfer bands (or bands arising from electronic transitions having partial charge transfer character) since in this case integrated intensity variations can be readily interpretable in terms of differing degrees of overlap between the molecular orbitals involved in the transition (Cordone et al. 1986); in this case, information on the temperature dependence of metal-ligand relative positions, i.e. on deformations of the active site that occur when the temperature is varied, can be obtained. Conversely, the observation of large temperature induced integrated intensity variations can give hints towards band assignment

Moreover, in (13) $P(n,T) = \prod_j p(n_j,T)$ with:

$$p(n_j,T) = \frac{e^{-\left(n_j+\frac{1}{2}\right)\frac{h\nu_j}{K_B T}}}{\sum_{n_j=0}^{\infty} e^{-\left(n_j+\frac{1}{2}\right)\frac{h\nu_j}{K_B T}}} = 2e^{-\left(n_j+\frac{1}{2}\right)\frac{h\nu_j}{K_B T}} \sinh\frac{h\nu_j}{2K_B T} \tag{15}$$

The optical absorption band profile is therefore given by:

$$F(\nu) = M\nu \sum_{\{m_j,n_j\}} \left[\prod_{j=1}^{N} \left| \int_{-\infty}^{\infty} \theta^*_{j,m_j}(q_j - \Delta_j)\,\theta_{j,n_j}(q_j)\,dq_j \right|^2 p(n_j,T)\right] \cdot \frac{\Gamma}{\left[\nu - \nu_{00} - \sum_i (m_j - n_j)\nu_j\right]^2 + \Gamma^2}. \tag{16}$$

We note that the temperature dependence of $F(\nu)$ is determined by the Boltzman factor $p(n_j,T)$: indeed, by increasing the temperature, the relative weight of anti-Stokes lines with $n_j > m_j$ increases and, in turn, this is reflected in a broadening of the band.

By expressing the Lorentzian in Eq. (16) as its Fourier transform, one has:

$$\begin{aligned} F(\nu) &= \frac{1}{2} M\nu \int_{-\infty}^{\infty} dt \sum_{\{m_j,n_j\}} \left[\prod_{j=1}^{N} \left| \int_{-\infty}^{\infty} \theta^*_{j,m_j}(q_j - \Delta_j)\,\theta_{j,n_j}(q_j)\,dq_j \right|^2 p(n_j,T)\right] \\ &\quad \times e^{-\Gamma|t|} \times e^{-i(\nu-\nu_{00})t} \times e^{i\sum_j (m_j-n_j)\nu_j t} \\ &= \frac{1}{2} M\nu \int_{-\infty}^{\infty} dt\, e^{-\Gamma|t|}\, e^{-i(\nu-\nu_{00})t} \\ &\quad \times \prod_{j=1}^{N_j} \sum_{\{m_j,n_j\}} \left| \int_{-\infty}^{\infty} \theta^*_{j,m_j}(q_j - \Delta_j)\,\theta_{j,n_j}(q_j)\,dq_j \right|^2 \end{aligned} \tag{17}$$

The term that has to be calculated is:

$$\prod_{j=1}^{N_j} \left[\sum_{\{m_j,n_j\}} \left| \int_{-\infty}^{\infty} \theta^*_{j,m_j}\left(q_j - \Delta_j\right)\theta_{j,n_j}(q_j)\,dq_j \right|^2 \cdot p(n_j,T) \times e^{i(m_j-n_j)\nu_j t}\right] \tag{18}$$

Using for $p(n_j,T)$ (15) and expressing $|\int \theta^*(q-\Delta)\,\theta(q)\,dq|^2$ as $\iint \theta(q)\theta^*(q')\,\theta^*(q-\Delta)\,\theta(q'-\Delta)\,dq\,dq'$, one can readjust expression (18) as:

$$\prod_{j=1}^{N_j} 2\sinh\frac{\beta_j}{2} \int_{-\infty}^{\infty}\int_{-\infty}^{\infty} \left[\sum_{m_j} \theta_{j,m_j}(q_j)\,\theta_{j,m_j}(q'_j) \times e^{-\left(m_j+\frac{1}{2}\right)\mu_j}\right] \times \left[\sum_{n_j} \theta_{j,n_j}(q_j - \Delta_j)\,\theta_{j,n_j}(q'_j - \Delta_j) \times e^{-\left(n_j+\frac{1}{2}\right)\lambda_j}\right] dq_j\,dq'_j \tag{19}$$

where $\beta_j = h\nu_j/K_B T$, $\lambda_j = \beta_j + i\nu_j t$ and $\mu_j = -i\nu_j t$.

Making use of Mehler's formula (Markham 1959) and of the properties of the harmonic oscillator eigenfunctions, after suitable manipulation it is possible to write the expression (19) as:

$$\prod_{j=1}^{N_j} \exp\left\{-S_j\left[\coth\left(\frac{\beta_j}{2}\right)\times(1-\cos\nu_j t)-i\sin\nu_j t\right]\right\} \quad (20)$$

where S_j is the linear coupling constant of the j-th vibrational mode ($S_j=(h/2)\,\nu_j(b)\,\Delta_j^2$) and where, of course, $\coth(\beta_j/2)=2\langle n_j\rangle+1$, $\langle n_j\rangle$ being the average vibrational occupation number.

If the temperature dependence of the band profile is studied over a finite temperature interval, one can perform a separation into vibrational modes whose population changes with temperature (low frequency modes, that contribute to the broadening of the band), and vibrational modes not populated in the temperature range investigated (high frequency modes). These last modes will, of course, be those whose frequency ν_h is such that $h\nu_h \gg K_B T_{\max}$, $T_{\max}$ being the upper limit of the temperature interval studied. The distinction between high and low frequency modes can be better understood by considering that for the former set only transitions from $n_h=0$ to $m_h=0, 1, 2, \ldots$ etc. occur while, for the latter also transitions from $n_l=0, 1, 2, \ldots$ etc. to $m_l=0, 1, 2, \ldots$ etc. are relevant, depending upon the temperature.

Accordingly expression (20) can be put as:

$$\left[\prod_{h=1}^{N_h} \exp\left\{-S_h\left[\coth\left(\frac{\beta_h}{2}\right)\times(1-\cos\nu_h t)-i\sin\nu_h t\right]\right\}\right] \times\left[\prod_{l=1}^{N_l} \exp\left\{-S_l\left[\coth\left(\frac{\beta_l}{2}\right)\times(1-\cos\nu_l t)-i\sin\nu_l t\right]\right\}\right] \quad (21)$$

where the subscript h and l indicate terms relative to high and low frequency modes respectively.

Expression (21) can be simplified by considering that for high frequency modes the average vibrational occupation number $\langle n_h\rangle$ is 0 in the whole temperature range (i.e. term $\coth[\beta_h/2]=1$); therefore, we can write:

$$\prod_{h=1}^{N_h} \mathrm{e}^{-S_h\left[\coth\left(\frac{\beta_h}{2}\right)\times(1-\cos\nu_h t)-i\sin\nu_h t\right]} = \prod_{h=1}^{N_h} \mathrm{e}^{-S_h\left[1-\mathrm{e}^{i\nu_h t}\right]} = \prod_{h=1}^{N_h} \mathrm{e}^{-S_h} \sum_{m_h} \frac{S_h^{m_h}\mathrm{e}^{im_h\nu_h t}}{m_h!} = \sum_{m_h}\prod_{h=1}^{N_h} \mathrm{e}^{-S_h}\,\frac{S_h^{m_h}\mathrm{e}^{im_h\nu_h t}}{m_h!} \quad (22)$$

Moreover, for low frequency modes, owing to the presence of the damping factor $\mathrm{e}^{(-\Gamma|t|)}$ in Eq. (17), the exponentials contribute significantly to the integral only in the time interval $0 \div \Gamma^{-1}$; this enables one to expand $\cos[\nu_l t]$ and $\sin[\nu_l t]$ up to order t^2 (short times approximation, Chan and Page 1983) and to obtain:

$$\prod_{l=1}^{N_l} \mathrm{e}^{-S_l\left[\coth\left(\frac{\beta_l}{2}\right)\times(1-\cos\nu_l t)-i\sin\nu_l t\right]} = \prod_{l=1}^{N_l} \mathrm{e}^{iS_l\nu_l t}\,\mathrm{e}^{-S_l\coth\left(\frac{\beta_l}{2}\right)\nu_l^2 t^2/2}. \quad (23)$$

We think it relevant to note that, as pointed out in the paper by Chan and Page (1983) the short times approximation is based on the assumption that dephasing of the N_l non degenerate low frequency modes occurs during the effective lifetime of excited state and not on the assumption that each ν_l (and therefore the average value $\langle\nu\rangle$) is much smaller than Γ.

To minimize the number of adjustable parameters the low frequency modes can be treated within the framework of so-called Einstein model, which considers the coupling of the electronic transition (linear coupling constant S) with N_1 degenerate lattice modes of frequency $\langle\nu\rangle$ ("bath" of low frequency modes); accordingly expression (23) becomes:

$$\mathrm{e}^{iN_l S\langle\nu\rangle t}\,\mathrm{e}^{-N_l S\coth\left(\frac{h\langle\nu\rangle}{2K_B T}\right)\langle\nu\rangle^2 t^2/2}. \quad (24)$$

Inserting expressions (22) and (24) into Eq. (17), one obtains for the absorption lineshape the following expression:

$$\begin{aligned} F(\nu) &= \frac{1}{2}M\nu\int_{-\infty}^{\infty} \mathrm{d}t\,\mathrm{e}^{-\Gamma|t|}\,\mathrm{e}^{-i(\nu-\nu_{00})t}\left[\prod_h\sum_{m_h}\mathrm{e}^{-S_h}\,\frac{S_h^{m_h}\mathrm{e}^{im_m\nu_h t}}{m_h!}\right] \\ &\quad\times\mathrm{e}^{iN_l S\langle\nu\rangle t}\times\mathrm{e}^{-N_l S\coth\left(\frac{h\langle\nu\rangle}{2K_B T}\right)\langle\nu\rangle^2 t^2/2} \\ &= \frac{1}{2}M\nu\sum_{\{m_h\}}\prod_{h=1}^{N_h}\mathrm{e}^{-S_h}\,\frac{S_h^{m_h}}{m_h!}\int_{-\infty}^{\infty}\mathrm{d}t\,\mathrm{e}^{-\Gamma|t|} \\ &\quad\times\mathrm{e}^{-i\left(\nu-\nu_{00}-\sum_{h=1}^{N_h} m_h\nu_h-N_l S\langle\nu\rangle\right)t}\,\mathrm{e}^{-N_l S\coth\left(\frac{h\langle\nu\rangle}{2K_B T}\right)\langle\nu\rangle^2 t^2/2} \end{aligned} \quad (25)$$

Equation (25) shows that $F(\nu)$ is given by the anti Fourier transform of the product of two functions, one being the Fourier transform of a Lorentzian and the other the Fourier transform of a Gaussian with temperature dependent width. Therefore, according to the convolution theorem the absorption in the frequency domain can be written as:

$$\begin{aligned} F(\nu) &= M\nu\left[L(\nu)\otimes G(\nu)\right] \\ &= M\nu\left\{\sum_{\{m_h\}}\left[\prod_h^{N_h}\frac{S_h^{m_h}\,\mathrm{e}^{-S_h}}{m_h!}\right]\right. \\ &\quad\times\frac{\Gamma}{\left[\nu-\nu_{00}-N_l S_l\langle\nu\rangle-\sum_h^{N_h} m_h\nu_h\right]^2+\Gamma^2} \\ &\quad\left.\otimes\frac{1}{\varsigma(T)}\,\mathrm{e}^{-\frac{\nu^2}{2\varsigma(T)^2}}\right\} \end{aligned} \quad (26)$$

where the symbol $\otimes$ represents the convolution operator (i.e. $f(\nu)\otimes g(\nu)=\int \mathrm{d}\nu' f(\nu-\nu')\,g(\nu')$) and where

$$\varsigma^2(T) = N_l S\langle\nu\rangle^2\coth\frac{h\langle\nu\rangle}{2K_B T}. \quad (27)$$

Inspection of Eq. (26) shows that, when only linear coupling is present, the spectrum results from the superposition of a series of Voigtians (Gaussian convolutions of Lorentzians); there is one series for each high frequency

mode: within each series the Voigtians are spaced by quantities multiple of the vibrational mode frequency. As the temperature is increased, the width of the Gaussian term $G(\nu)$ increases (27), while the peak frequency remains constant. We recall that coupling with high frequency modes does not contribute to the temperature dependence of the bandwidth but only introduces a wing of Lorentzians centered at the various vibronic frequencies of the fundamental, while the temperature dependence of the bandwidth is brought about by coupling of the electronic transition with low frequency modes.

To take into account temperature effects on the peak position of the optical absorption bands, one has to consider that the electronic promotion not only causes a shift in the nuclear equilibrium positions (linear coupling) but also changes the vibrational frequencies (quadratic coupling); it can be shown (see Appendix A) that when quadratic coupling is taken into account the expression for the absorption becomes:

$$F(\nu) = M\nu\left[L(\nu)\otimes G(\nu)\right] = M\nu\left\{\sum_{\{m_h\}}\left[\prod_{h=1}^{N_h}\frac{S_h^{m_h}\,e^{-S_h}}{m_h!}\right] \times \frac{\Gamma}{\left[\nu-\nu_0(T)\right]^2+\Gamma^2}\otimes\frac{1}{\varsigma(T)}\,e^{-\frac{\nu^2}{2\varsigma^2(T)}}\right\} \quad (28)$$

with

$$\varsigma^2(T) = N_l\,S\,R_l^2\langle\nu\rangle^2\coth\frac{h\langle\nu\rangle}{2K_BT} \quad (29)$$

$$\nu_0(T) = \nu_{00} - \frac{1}{4}N_l(1-R_l)\langle\nu\rangle\coth\frac{h\langle\nu\rangle}{2K_BT} + C \quad (30)$$

In (29) and (30) the quantity R_l is the "effective" quadratic coupling constant of the electronic transition to the low frequency bath; moreover the term $C=\Sigma_h m_h R_h \nu_h(a) - 1/4\,\Sigma_h(1-R_h)\nu_h(a)+N_lSR_l\langle\nu\rangle$ takes into account the temperature independent contributions to the peak frequency arising from high and low frequency modes. The presence of quadratic coupling does not substantially influence the thermal broadening of the Gaussian linewidth but it introduces a temperature dependence of the peak frequencies of the Voigtians: a blue shift or a red shift of the spectrum will be observed by increasing temperature, for $R_l>1$ or $R_l<1$, respectively, (i.e. for $\langle\nu\rangle$ in the excited electronic state larger or smaller than $\langle\nu\rangle$ in the ground state).

Further contributions to the spectral lineshape are inhomogeneous effects arising from different conformational substates and heme group environments (Frauenfelder et al. 1988; Ormos et al. 1990). If such conformational heterogeneity is present, one has to perform averages over spectrally different species and this has two main consequences:

i) parameters like S_h, S, R_l, ν_h and $\langle\nu\rangle$ assume ensemble averaged values and
ii) the transition frequency ν_{00} becomes distributed.

We can therefore write for the absorption:

$$A(\nu) = M\nu\{[L(\nu)\otimes G(\nu)]\otimes P(\nu_{00})\} \quad (31)$$

where $P(\nu_{00})$ is the distribution function for ν_{00}, i.e. $P(\nu_{00})\,d\nu_{00}$ gives the probability of having a transition frequency between ν_{00} and $\nu_{00}+d\nu_{00}$. It should be stressed that $P(\nu_{00})$ is a spectral and not a conformational distribution function.

To obtain a conformational distribution function we assume that the geometry of our system (porphyrin+iron atom+iron ligands) can be described by two generalized non-correlated coordinates X and ϕ (Srajer and Champion 1991) that, in view of conformational heterogneity, will be statistically distributed, i.e. we write:

$$P(X,\phi) = P(X)\cdot P(\phi) = \frac{\exp\left[-(X-X_0)^2/2\delta_x^2\right]}{\sqrt{2\pi}\,\delta_x}\cdot\frac{\exp\left[-(\phi-\phi_o)^2/2\delta_\phi^2\right]}{\sqrt{2\pi}\,\delta_\phi} \quad (32)$$

where X_0 and ϕ_0 are the mean coordinate positions and δ_X and δ_ϕ the widths of the distributions. The coordinate X is expected to describe essentially the iron displacement out of the mean porphyrin plane (i.e. the value $X=0$ corresponds to the in plane iron position characteristic of the liganded heme proteins derivatives), while the coordinate ϕ represents other angular coordinates such as the proximal histidine tilt and/or azimuthal orientation or the angular position of the distal ligand with respect to the heme normal.

Since the energy of the $\pi\rightarrow\pi^*$ electronic transition responsible for the Soret band (purely electronic transition frequency, ν_{00}) depends upon the coordinate X and ϕ, the conformational heterogeneity is "mapped" into the spectral one. In general one has:

$$\nu_{00}(X,\phi) = \nu_{00}^* + a\,\phi + a'\,\phi^2 + bX^2 \quad (33)$$

with $\nu_{00}^* = \nu_{00}\big|_{(X=0,\,\phi=0)}$ and where higher order terms have been neglected. It should be noted that, in view of the approximate reflection symmetry of the iron-porphyrin system, only even terms are retained in the dependence of ν_{00} upon X. To proceed further we will consider separately the cases of liganded and unliganded hemeproteins.

Case a): liganded hemeproteins

In this case (typical example: CO derivatives) the iron atom is locked into the heme plane by the liganded CO molecule ($X_0=0$) and its distribution is so narrow that $P(X)$ can be considered as a delta function; moreover, the average value of the angular coordinate ϕ can be taken as $\phi_0=0$ and quadratic contributions to $\nu_{00}(\phi)$ can be neglected, so that (32) and (33) become:

$$P(\phi) = \frac{\exp\left[-\phi^2/2\delta_\phi^2\right]}{\sqrt{2\pi}\,\delta_\phi} \quad (34)$$

$$\nu_{00}(\phi) = \nu_{00}^* + a\,\phi \quad (35)$$

Combining (34) and (35) one obtains for the spectral heterogeneity:

$$P(\nu_{00}) = \frac{1}{\sqrt{2\pi}\, a\,\delta_\phi}\, e^{-\frac{\left[\nu_{00}-\nu_{00}^*\right]^2}{2a^2\delta_\phi^2}} \tag{36}$$

and for the absorption as a function of frequency:

$$\begin{aligned} A(\nu) &= M\nu\left\{\left[L(\nu)\otimes G(\nu)\right]\otimes \frac{1}{\sqrt{2\pi}\, a\,\delta_\phi}\, e^{-\frac{\left[\nu_{00}-\nu_{00}^*\right]^2}{2a^2\delta^2}}\right\} \\ &= M\nu\left[L(\nu)\otimes \frac{1}{\sigma(T)}\, e^{-\frac{\nu^2}{2\sigma^2(T)}}\right] \\ &= M\nu\left[L(\nu)\otimes G'(\nu)\right] \end{aligned} \tag{37}$$

where now the temperature dependent width of the Gaussian term $G'(\nu)$ is given by

$$\sigma^2(T) = N_l\, S\, R_l^2 \langle\nu\rangle^2 \coth\frac{h\langle\nu\rangle}{2K_B T} + \sigma_{\text{in}}^2 \tag{38}$$

being $\sigma_{\text{in}}^2 = a^2\,\delta_\phi^2$; moreover the term $G'(\nu)$ differs from $G(\nu)$ only for constant terms arising from the normalization factors of the probability function.

Therefore it can be seen that in the case of liganded derivatives inhomogeneous broadening due to conformational heterogeneity simply adds to the Gaussian width a temperature independent term (σ_{in}^2).

Case b): unliganded hemeproteins

In this case the iron atom lies out of the mean porphyrin plane ($X_0 \neq 0$) and is more loosely bound so that the disorder in its out of plane displacement may be substantial. Since the iron d electrons interact strongly with the π electrons of the porphyrin ring and in view of the absence of a distal iron ligand, we can neglect the dependence of ν_{00} upon the coordinate ϕ so that (33) becomes (Srajer et al. 1986):

$$\nu_{00}(X) = \nu_{00}^* + b\,X^2 \;\Rightarrow\; X = \pm\sqrt{\left[\nu_{00}-\nu_{00}^*\right]/b} \tag{39}$$

Combining (33) and (39) one obtains:

$$P(\nu_{00}) = \frac{e^{-\frac{\left[\sqrt{\nu_{00}-\nu_{00}^*}+X_0\sqrt{b}\right]^2}{2b\delta_x^2}} + e^{-\frac{\left[\sqrt{\nu_{00}-\nu_{00}^*}-X_0\sqrt{b}\right]^2}{2b\delta_x^2}}}{2\delta_x\sqrt{2\pi b\left[\nu_{00}-\nu_{00}^*\right]}} \tag{40}$$

From (40) it can be seen that for unliganded hemeproteins derivatives a Gaussian distribution of iron atom out of plane positions produces an asymmetric non-Gaussian distribution of electronic transition energies; this effect, that is mainly due to the position of the iron atom out of the mean porphyrin plane, is responsible for the characteristic marked asymmetry of the Soret band of deoxy hemeproteins.

The expression for the absorption as a function of frequency, suitable to analyze the deoxy spectra therefore becomes:

$$A(\nu) = M\nu\left\{\left[L(\nu)\otimes G(\nu)\right] \otimes \frac{e^{-\frac{\left[\sqrt{\nu_{00}-\nu_{00}^*}+X_0\sqrt{b}\right]^2}{2b\delta_x^2}} + e^{-\frac{\left[\sqrt{\nu_{00}-\nu_{00}^*}-X_0\sqrt{b}\right]^2}{2b\delta_x^2}}}{2\delta_x\sqrt{2\pi b\left[\nu_{00}-\nu_{00}^*\right]}}\right\} \tag{41}$$

In (41) X_0 and δ_X are the average out of plane iron displacement and its disorder parameter, whereas b is a proportionality constant between the $\pi\rightarrow\pi^*$ transition energy and the iron position; it should be stressed that only the quantities $X_0\sqrt{b}$ and $\delta_X\sqrt{b}$ (and not X_0 or δ_X) can be obtained by fitting the experimental spectra. It should be noted also that the term σ_{in}^2 does not appear in the temperature dependence of the Gaussian width of the deoxy spectra since the effect of inhomogeneous broadening is taken into account by the parameter $\delta_X\sqrt{b}$.

The various contributions to the Soret band lineshape of SwMb-CO are represented in Fig. 3 where experimental data measured at 20 K are reported as dots (after subtracting contributions from the N band), while solid lines represent partially or totally reconstructed spectra. Panel 3a shows the purely Lorentzian spectrum of the isolated chromophore (4); the effect of coupling with high frequency nuclear motions is shown in panels 3b and 3c (to better demonstrate the effect of coupling to high frequency modes the reconstructed spectrum in panel 3b is a "high resolution spectrum" obtained using an homogeneous width Γ one half of the suitable value); the further effect of coupling with a "bath" of low frequency modes and of a Gaussian inhomogeneous broadening is shown in panel 3d where the fitting of the experimental points is shown.

The same contributions are reported in Fig. 4 for the Soret band of SwMb. In panel 4c only the effect of coupling with a "bath" of low frequency modes is considered: as can be seen, the introduction of only Gaussian broadening is clearly not adequate to account for the marked asymmetry of the band; in contrast, further addition of an asymmetric non-Gaussian inhomogeneous broadening (41) reported in panel 4d, results in an excellent fitting. The values of the parameters used to generate the theoretical spectra in Figs. 3 and 4 are reported in Table 1.

A practical limitation in performing the spectral deconvolution we report lies on the rather large number of fitting parameters that can hardly be unambiguously determined. This difficulty, however, can be circumvented for the Soret band of hemeproteins since:

i) one has to deal with a single well defined band clearly assigned to a single $\pi\rightarrow\pi^*$ electronic transition (Eaton et al. 1978; Eaton and Hofrichter 1981; Makinen and Churg 1983);
ii) vibrational frequencies of "high frequency modes" are known from resonance Raman measurements (Asher 1981; Bangcharoenpaurpong et al. 1984; Tsubaki et al. 1982);
iii) the presence of a clearly resolved vibronic structure (at least at low temperatures) enables one to obtain the

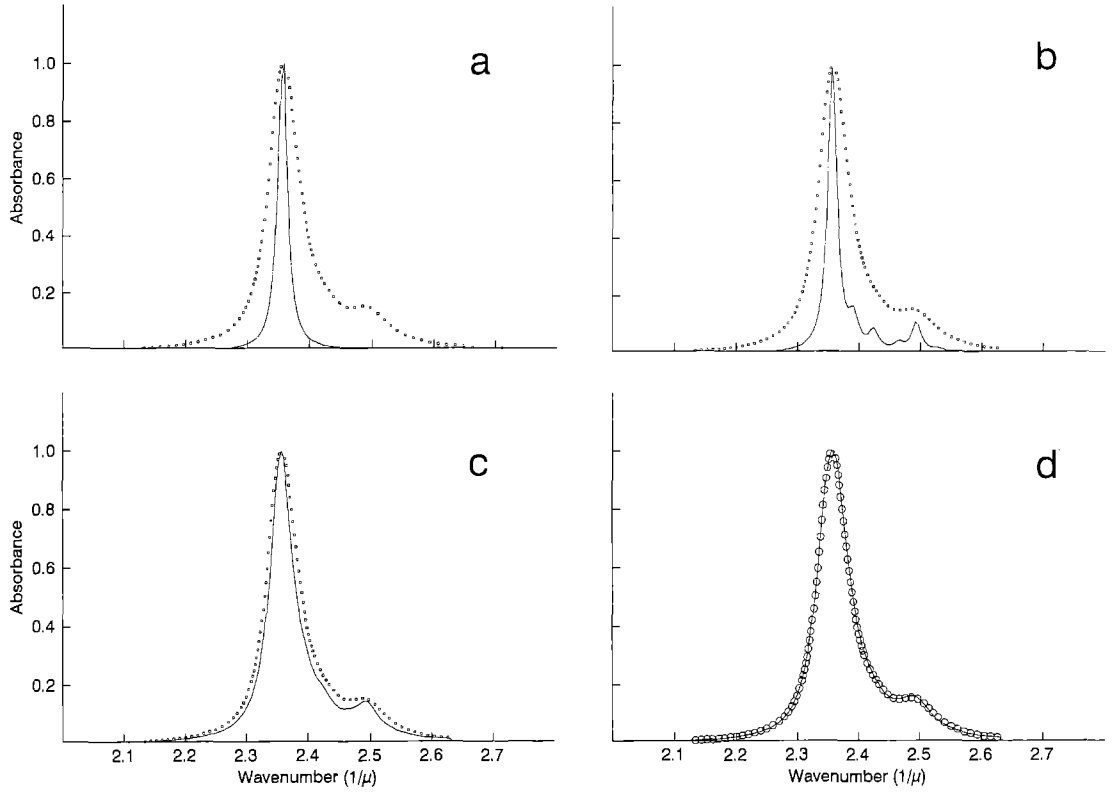

Fig. 3a–d. Comparison of calculated and experimental Soret band profiles at $T=20$ K for SWMb-CO. Dots represent the experimental data, after subtraction of the higher frequency N band; solid lines represent the calculated spectra. **a** Purely Lorentzian profile ($\Gamma=90$ cm^{-1}). **b** Lorentzian profile + coupling with high frequency modes; to evidence the vibronic coupling a Γ value of 90 cm^{-1} has been used. **c** As in panel b with $\Gamma=211$ cm^{-1}. **d** Lorentzian profile + vibronic coupling + low frequency modes + Gaussian inhomogeneous broadening. Values of the parameters relative to the theoretical profiles are given in Table 1

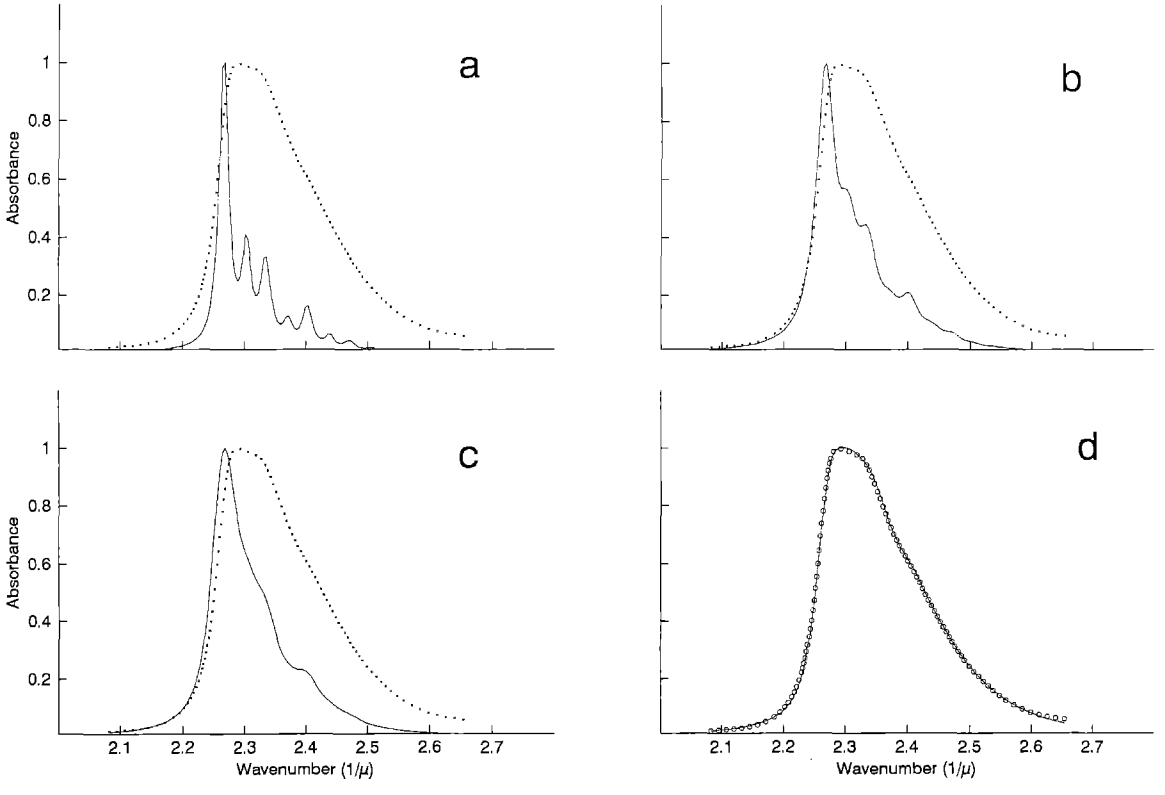

Fig. 4a–d. As in Fig. 3, SWMb. **a** Lorentzian profile + coupling with high frequency modes; to show the vibronic coupling a Γ value of 90 cm^{-1} has been used. **b** As in panel a with $\Gamma=180$ cm^{-1}. **c** Lorentzian profile + vibronic coupling + low frequency modes. **d** Lorentzian profile + vibronic coupling + low frequency modes + non Gaussian asymmetric inhomogeneous broadening. Values of the parameters relative to the theoretical profiles are given in Table 1

Table 1. Low temperature (T=20 K) linear coupling constants of the high frequency modes, Γ and σ values for SWMb and SWMbCO

	S_{370}	S_{674}	S_{1100}	S_{1357}	σ/cm^{-1}	Γ/cm^{-1}
SWMb	0.32±0.02	0.24±0.02	<0.01	0.10±0.01	95	180±10
SWMbCO	0.12±0.02[a]	0.06±0.01[b]	0.02±0.008	0.09±0.01[c]	115	211± 7

[a] Data relative to SWMbCO refer to the mode at 350 cm^{-1}
[b] Data relative to SWMbCO refer to the mode at 676 cm^{-1}
[c] Data relative to SWMbCO refer to the mode at 1374 cm^{-1}

values of linear coupling constants S_h; moreover, for hemeproteins, S_h values are also available from independent Raman excitation profiles measurements (Bangcharoenpaurpong et al. 1984; Morikis et al. 1991; Schomacker and Champion 1986, 1989; Schweitzer-Stenner et al. 1992, 1993);

iv) the well defined red edge of the band enables an unambiguous determination of the Lorentzian width; separation of the Gaussian (σ) from the Lorentzian width (Γ) can be, in fact, a major problem when dealing with less well resolved bands.[4]

When the band profile is not clearly ascribed to a single electronic transition (partially overlapping bands) or when the vibronic structure is not clearly resolved, the method outlined above is not applicable. Information on the effect of coupling with low frequency modes, however, can be obtained together with some information on dynamic properties of the system through the simplified "Methods of moments", described in Appendix B.

Some experimental results

In this section we review some already published results on the dynamic properties of the heme pocket in liganded (CO derivatives) and unliganded spermwhale myoglobin, obtained by applying the above approach to the analysis of the Soret band absorption spectra in the temperature range 300–20 K.

Figure 5 shows the 20 K spectra of carbonmonoxy and deoxy derivatives of spermwhale myoglobin (SWMbCO and SWMb, respectively), together with the fittings obtained using (37) (CO derivative) and (41) (deoxy derivative); the residuals are also shown on expanded scales. Values of the parameters in (37) and (41), obtained from fittings, are reported in Table 1.

We will concentrate on the temperature dependence of parameter σ^2 (the Gaussian broadening of the band) since this gives information on the low frequency bath that characterizes the soft motions likely involving large parts of the protein (for a detailed discussion on the other fitting parameters see e.g. Di Pace et al. 1992; Cupane et al. 1993a).

The σ^2 temperature dependence relative to SWMbCO and SWMb is reported in Fig. 6. It is evident that Eq. (38) cannot suitably fit the experimental σ^2 values in the whole temperature range 20–300 K. In fact, the limiting behavior of the hyperbolic cotangent in (38) for $K_B T \gg <\nu>/2$ is a straight line whose intercept at T=0 represents σ^2_{in} that, of course, cannot be negative. The high temperature σ^2 behavior must therefore be represented by a straight line having positive (or 0, for the deoxy derivative) intercept at T=0. The fact that in Fig. 6 the straight line tangent to the high temperature experimental points has a negative intercept at T=0 implies therefore that (38), and the harmonic model on which it is based, cannot account for the thermal evolution of the bandwidth in the whole temperature range explored. Physically meaningful fitting of (38) to the experimental data can, however, be performed in the range 20–160 K (CO derivative) and 20–110 K (deoxy derivative); these fittings are shown by the continuous lines in Fig. 6. The relative fitting parameters are reported in Table 2.

$\Delta\sigma^2$ values, i.e. the differences between the experimental points and the continuous lines in Fig. 6, are reported in Fig. 7. Since, as mentioned above, (38) has been derived within the harmonic approximation, we suggested that $\Delta\sigma^2$ reflect the onset of non-harmonic contributions in the nuclear motions coupled to the electronic transition. These motions could involve torsional degrees of freedom and the jumping of nuclei between different minima of the torsional potential ("torsional jumping") (Elber and Karplus 1987; Frauenfelder et al. 1988) and/or a softening, at temperatures above that of the solvent glass transition, of the average frequency of the "low frequency bath" that would indeed cause an amplitude increase of the nuclear motions above that predicted by the harmonic behavior (Levy et al. 1982).

Data in Fig. 7 show that anharmonic contributions depend on the state of ligation of the protein: indeed for the deoxy derivative deviations from the harmonic behavior

[4] In some experimental cases the red edge of the absorption band appears to be almost perfectly Gaussian, owing to the fact that the value of the parameter Γ is very small with respect to experimental linewidth. In this case, if a clearly defined vibronic structure, due to the coupling with high frequency modes, is present (see Leone et al. 1992) one can approximate the Lorentzian in (26) with a delta function obtaining:

$$G(\nu)=M\nu\sum_{m_h}\left\{\left[\prod_{h=1}^{N_h}\frac{S_h^{m_h}e^{-S_h}}{m_h!}\right]\times\frac{1}{\varsigma(T)}e^{-\frac{\left[\nu-\nu_0(T)-\sum_h m_h\nu_h-N_l S_l\langle\nu\rangle\right]^2}{2\varsigma^2(T)}}\right\}$$

where $\varsigma^2(T)$ is again given by Eq. (29).

In this case therefore the spectrum results from a superposition of a series of Gaussians centered at the various vibronic frequency of the fundamental. Starting from the above expression, the effects of quadratic coupling and of inhomogeneous broadening can be treated as described in the text

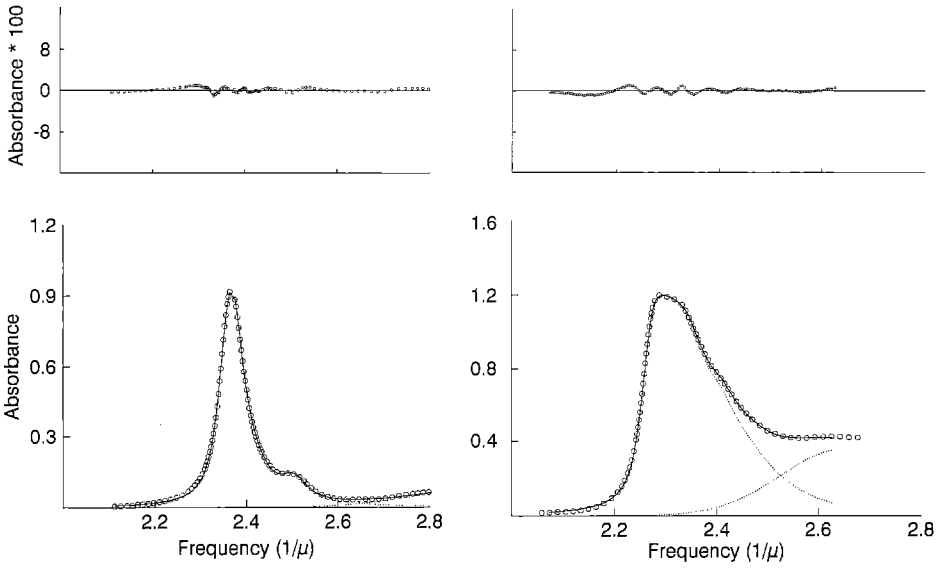

Fig. 5. Soret spectra of SWMbCO (*left*) and of SWMb (*right*) at $T=20$ K. Protein concentrations are $\approx 4\times10^{-6}$ M for SWMbCO and $\approx 9\times10^{-6}$ M for SWMb; other experimental conditions as in Fig. 1. Circles are the experimental points; dotted lines represent the fittings in terms of (37) (SWMbCO) and (41) (SWMb) and contributions from the N band; the overall synthesized band profiles are given by the continuous lines. For the sake of clarity, not all the experimental points have been reported. The residuals are also shown in the upper panels, on expanded scales

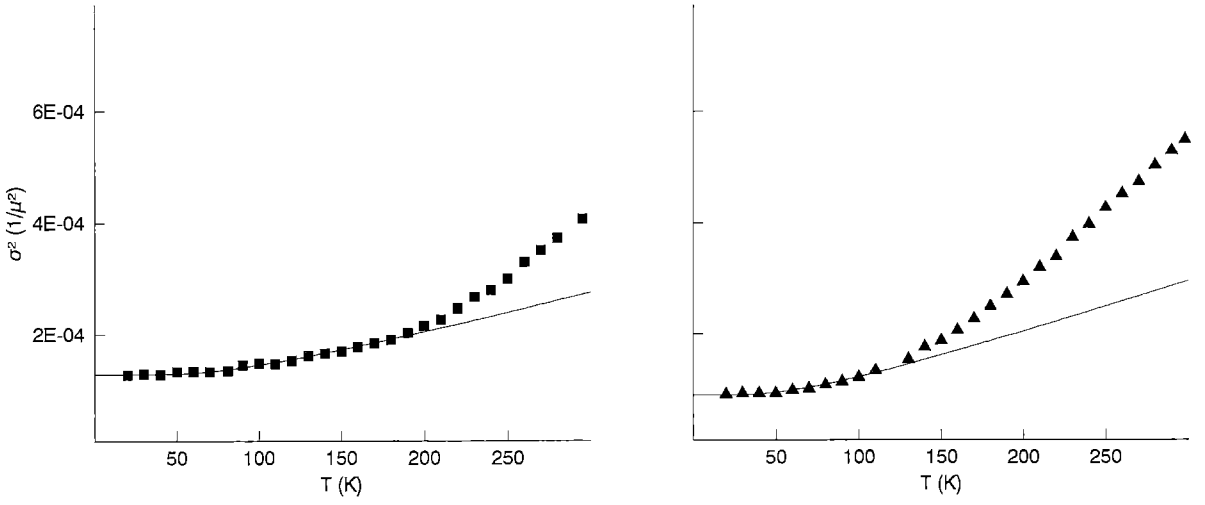

Fig. 6. Temperature dependence of the Gaussian width (σ^2) of the Soret band of SWMbCO (*squares, left panel*) and of SWMb (*triangles, right panel*). The continuous lines represent fittings of the data in the temperature range 20–160 K (CO derivatives) and 20–110 K (deoxy derivatives) in terms of (38). For the deoxy derivative a value of $\sigma^2_{in}=0$ has been used (see text)

Table 2. Values of the parameters obtained by fitting the ν_0 and σ^2 behavior in the temperature range 20–110 K in terms of (30) and (38), taken from Cupane et al. 1993 b

	$N_1 S$ [a]	σ_{in}/cm^{-1}	$\langle\nu\rangle/cm^{-1}$	R [b]	$(\nu_{00}(Q=0)+C)/cm^{-1}$
SWMb	0.5±0.1	–	132±10	1.02±0.004	22.629±2
SWMbCO	0.3±0.2	53±38	180±30	1.01±0.002	23.567±4

[a] $N_1 S$ values are obtained under the assumption $R^2\approx 1$

[b] R_1 values are obtained by assuming the coupling with $N=50$ low frequency modes

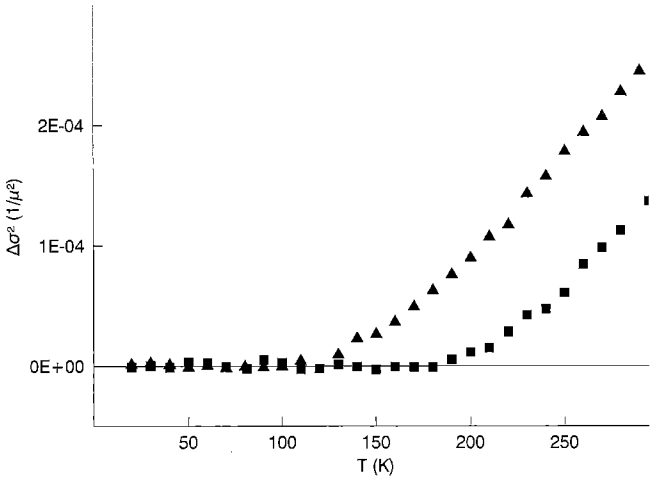

Fig. 7. Differences between σ^2 values and calculated harmonic behavior as a function of temperature. *Squares:* SWMbCO; *triangles:* SWMb

start at a lower temperature and are larger in magnitude than those relative to the CO derivative. This observation points out the stabilizing effect of the bound CO molecule on the dynamics of the heme pocket in myoglobin. It is also tempting to speculate on the possible functional role of the above effects: in fact, anharmonicity of nuclear motions is an obvious prerequisite for the jumping among different conformational substates of the protein that, in turn, is necessary e.g. to open "channels" for the ligands to reach the active site in this protein (Case and Karplus 1978; Keller and Debrunner 1980; Debrunner and Frauenfelder 1982; Ansari et al. 1986).

Finally, it should also be mentioned that for various myoglobin derivatives, an increase in the average atomic fluctuations of the iron, of backbone and side-chains atoms and of hydrogen atoms well above the predictions of the harmonic behavior and occurring at temperatures higher than 180 K has been observed both experimentally, by Mossbauer spectroscopy (Mb and Mb^{3+} crystals, Parak et al. 1981, 1982) and inelastic neutron scattering (Mb^{3+} hydrated powders, Doster et al. 1989; Cusack and Doster 1990), and by computer simulations (MbCO, Loncharich and Brooks 1990; Smith et al. 1990); this effect has been attributed to a transition (occurring at about 200 K) in protein mobility from the low temperature "solid like" behavior characterized by essentially harmonic oscillations of the nuclei around their equilibrium positions to a high temperature "liquid-like" behavior characterized by the jumping between different conformational substates of the protein.

Acknowledgements. The authors wish to tank Dr. R. Passante for helpful discussions and for a critical readingof the manuscript. This work has been supported by grants from "Ministero dell'Università e della Ricerca Scientifica". General indirect support from Sicilian "Comitato Regionale Ricerche Nucleari e Struttura della Materia" is also acknowledged.

Appendix A

This appendix reports the effects of electron-vibrations quadratic coupling on the temperature dependence of absorption lineshape.

We recall that the energies of the ground (a) and excited states (b) are given by (see (5)–(7) in the text):

$$E_a = \eta_a + \frac{1}{2} h^2 \sum_{j=1}^{N} \nu_j^2(a)\, q_j^2 ;$$

$$E_b = \eta_b + \Delta E_0 + \sum_{j=1}^{N} \alpha_j\, q_j + \frac{1}{2} \sum_{j=1}^{N} [\alpha_{jj} + h^2\, \nu_j^2(a)]\, q_j^2 .$$

Introducing the quadratic coupling constants $R_j = \nu_j^2(b)/\nu_j^2(a)$, we can rewrite E_b and E_b as:

$$E_b = \eta_a + \Delta E_0 + \sum_{j=1}^{N} \alpha_j\, q_j + \frac{1}{2} h^2 \sum_{j=1}^{N} R_j^2\, \nu_j^2(a) \left(\frac{Q_j}{\sqrt{R_j}} \right)^2 \tag{A1}$$

$$\begin{aligned} E_a &= \eta_a + \frac{1}{2} h^2 \sum_{j=1}^{N} R_j^2\, \nu_j^2(a) \left(\frac{q_j}{\sqrt{R_j}} \right)^2 + \frac{1}{2} h^2 \sum_{j=1}^{N} R_j [\nu_j^2(a) - \nu_j^2(b)] \left(\frac{q_j}{\sqrt{R_j}} \right)^2 \\ &= \eta_a + \frac{1}{2} h^2 \sum_{j=1}^{N} \nu_j^2(a)\, [R_j^2 + R_j(1 - R_j)] \left(\frac{q_j}{\sqrt{R_j}} \right)^2 \end{aligned} \tag{A2}$$

By considering that $|\nu_j^2(a) - \nu_j^2(b)| \ll \nu_j^2(a)$ and therefore that $|1 - R_j| \ll R_j$, one obtains:

$$\begin{aligned} \left(\frac{E_b - E_a}{h} \right) &= \nu_{00} + \sum_{j=1}^{N} R_j \left(m_j + \frac{1}{2} \right) \nu_j(a) - \sum_{j=1}^{N} R_j \left(n_j + \frac{1}{2} \right) \nu_j(a) - \frac{1}{2} \sum_{j=1}^{N} (1 - R_j) \left(n_j + \frac{1}{2} \right) \nu_j(a) \\ &= \nu_{00} + \sum_{j=1}^{N} R_j (m_j - n_j)\, \nu_j(a) - \frac{1}{2} \sum_{j=1}^{N} (1 - R_j) \left(n_j + \frac{1}{2} \right) \nu_j(a) . \end{aligned} \tag{A3}$$

Substituting the last term of Eq. (A3) with its average value one has:

$$\left(\frac{E_b - E_a}{h} \right) = \nu_{00} + \sum_{j=1}^{N} R_j (m_j - n_j)\, \nu_j(a) - \frac{1}{4} \sum_{j=1}^{N} (1 - R_j)\, \nu_j(a)\, (2 \langle n_j \rangle + 1) \tag{A4}$$

Equations (A1), (A2) and (A4) are formally identical to Eqs. (6), (5) and (8) respectively, provided that:

i) the quantities $R_j\, v_j(a)$, $Q_j/\sqrt{R_j}$ and $q_j/\sqrt{R_j}$ are substituted for v_j, Q_j and q_j respectively;
ii) the temperature dependent term $-1/4 \sum_j (1-R_j)\, v_j(a)\, (2\langle n_j\rangle+1)$ is added to v_{00}.

The procedure to calculate the absorption lineshape therefore runs exactly as described in the text and (28), (29) and (30) are straightforwardly obtained.

Appendix B

Optical spectra of metalloproteins often arise from several electronic transitions occurring in a rather narrow frequency range and therefore consist of several, partially overlapping, bands. In these situations the red edge of the bands and their vibronic structure remain unresolved even at very low temperatures and therefore attempts at analyzing the measured spectra in terms of Eqs. (37) or (41) are hopeless. Some information on the dynamics of the system, however, can be obtained through the "Method of moments". To this purpose the measured spectra at various temperatures are heuristically deconvoluted in terms of Gaussian components:

$$A(v) = \sum_j a_j \exp\left[-\frac{(v-v_{0j})^2}{2\sigma_j^2}\right] \tag{B1}$$

where a_j, v_{0j} and σ_j are the intensity, peak frequency and halfwidth of each component j. Each Gaussian identifies a spectral band; however, when two or more components are so near that they are not resolved separately in the spectrum even at low temperature, a single "band" arising from their sum is considered. Thereafter, the zeroth (M_0), first (M_1) and second (M_2) moment of each "band" is calculated, within the so called narrow band approximation (Dexter 1958), according to the definitions given by Markham (1959), i.e.:

$$M_0 = \int_{-\infty}^{\infty} \varepsilon(v)\, dv;$$

$$M_1 = \frac{1}{M_0} \int_{-\infty}^{\infty} v\, \varepsilon(v)\, dv;$$

$$M_2 = \frac{1}{M_0} \int_{-\infty}^{\infty} v^2\, \varepsilon(v)\, dv - M_1^2 \tag{B2}$$

where $\varepsilon(v)$ is the absorbance, at frequency v, of the distribution that takes into account the band of interest. We recall that M_0 represents the integrated intensity of the band, M_1 its average frequency and M_2 its width; moreover, for purely Gaussian bands,

$$M_0 = \sqrt{2\pi}\, a\sigma; \quad M_1 = v_0; \quad M_2 = \sigma^2. \tag{B3}$$

Approximate expressions for the temperature dependence of M_1 and M_2 have been derived by Markham (1959):

$$M_1 = D + F \coth\frac{h\langle v\rangle}{2K_B T}; \quad M_2 = A \coth\frac{h\langle v\rangle}{2K_B T} + C^2 \tag{B4}$$

where the parameter $\langle v\rangle$ is a "mean effective" frequency of the bath of nuclear motions coupled to the electronic transition responsible for the band investigated. The term C^2 takes into account all temperature independent contributions to linewidth that are not resolved from the analysis, i.e. homogeneous broadening (Lorentzian width Γ), coupling with high frequency modes not populated in the temperature range investigated and inhomogeneous broadening; analogous contributions to M_1 are included in the parameter D.

As an example, we show in Fig. 8 the procedure followed to analyze the temperature dependence of the visible bands of azurin (Cupane et al. 1990 a, b). In the left panel of Fig. 8 the low temperature (T=20 K) visible spectrum is reported, together with the fitting in terms of Gaussian components. Four bands, attributed to ligand to metal charge transfer transitions, are expected (Solomon et al. 1980; McMillin and Morris 1981; Gewirth and Solomon 1988) and, indeed, four Gaussian components (labeled I to IV in Fig. 8) are needed to fit the spectrum. However, bands II and III are not resolved separately, even at low temperature; for this reason, we considered a single "band" arising from the sum of bands II and III and calculated the moments of this "bands" from the distribution resulting from the sum of the Gaussian components II and III. The temperature dependence of M_2 is shown in the right panel of Fig. 8 together with the fitting in terms of (B1). The value of the parameter $\langle v\rangle$ obtained (and confirmed by the analysis of band I) is about 150 cm^{-1} and this fact points out the coupling of low frequency ligand-metal-ligand deformation modes with the copper orbitals that, in turn, are directly involved in the biological function of the protein. A role of the above low frequency modes on the electron transfer process could therefore be inferred from the study.

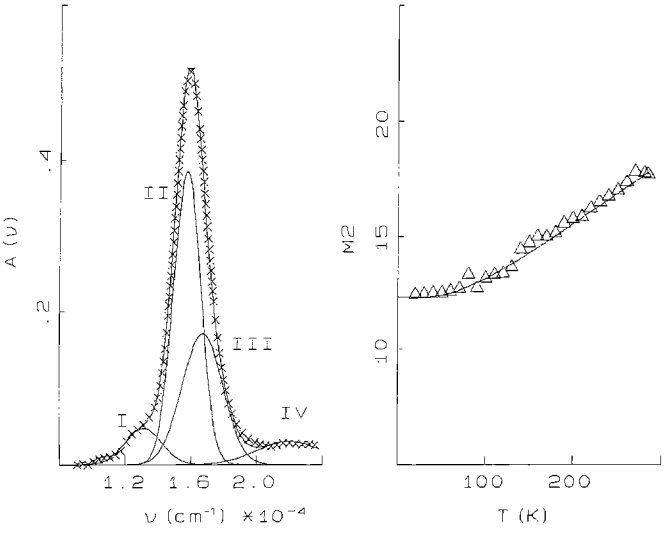

Fig. 8. *Left:* deconvolution of the 20 K absorption spectrum of azurin in terms of Gaussian components; protein concentration is $\approx 1.2\times10^{-4}$ M, other experimental conditions as in Fig. 1; the crosses represent the experimental points; continuous lines represent the Gaussian components and the synthesized band profile; for the sake of clarity, not all the experimental points have been reported. *Right:* second moment (M_2) of band II + III of azurin as a function of temperature; the continuous line represents the best fit of (B4) to the experimental points; the M_2 scale is $cm^{-2}\times10^{-5}$

The main advantage of the method lies in the fact that one does not need any detailed theoretical expression for the spectral lineshape; in fact, the deconvolution of the spectra into Gaussian components is an heuristic one and is performed only in order to calculate the moments of the bands. The most severe limitation is that only average information on the stereodynamic properties of the system under study can be obtained; in particular, the fact that relevant lineshape contributions (homogeneous broadening, vibronic coupling with high frequency modes, conformational heterogeneity) are not sorted out separately but added as constant terms to the M_2 temperature dependence could mask important dynamic effects.

References

Allendorf MD, Spira DJ, Solomon EI (1985) Low temperature magnetic circular dichroism studies of native laccase: spectroscopic evidence for exogenous ligand bridging at a trinuclear copper active sire. Proc Natl Acad Sci, USA 82:3063–3067

Ansari A, Di Iorio EE, Dlott DD, Frauenfelder H, Iben IET, Langer P, Roder H, Sauke TB, Shyamsunder E (1986) Ligand Binding to hemeproteins: Relevance of low-temperature data. Biochemistry 25:3139–3146

Asher SA (1981) Resonance Raman spectroscopy of hemoglobin. Methods Enzymol 76:371–413

Bangcharoenpaurpong O, Schomacker KT, Champion PM (1984) A resonance Raman investigation of myoglobin and hemoglobin. J Am Chem Soc 106:5688–5698

Bransden BH, Joachain CJ (1983) In: Physics of atoms and molecules. J. Wiley & Sons, New York

Browett WR, Stillman MJ (1984) Temperature dependence of the absorption spectra of beef liver catalase. Biophys Chem 19: 311–320

Case DA, Karplus M (1978) Stereochemistry of carbonmonoxide binding to myoglobin and hemoglobin. J Mol Biol 123:697–701

Chan CK, Page JB (1983) Temperature effects in the time correlator theory of resonance raman scattering. J Chem Phys 79: 5234–5250

Cordone L, Cupane A, Leone M, Vitrano E (1986) Optical absorption spectra of deoxy- and oxyhemoglobin in the temperature range 300–20 K: relation with protein dynamics. Biophys Chem 24:259–275

Cordone L, Cupane A, Leone M, Vitrano E, Bulone D (1988) Interaction between external medium and haem pocket in myoglobin probed by low-temperature optical spectroscopy. J Mol Biol 198: 213–218

Cupane A, Leone M, Vitrano E, Cordone L (1988) Structural and dynamic properties of the heme pocket in myoglobin probed by optical spectroscopy. Biopolymers 27:1977–1997

Cupane A, Leone M, Vitrano E, Cordone L (1990 a) Dynamic properties of the active site of azurin studied by the temperature dependence of the optical spectrum. Biol Metals 3:77–79

Cupane A, Leone M, Vitrano E, Cordone L (1990 b) Optical absorption spectra of azurin and stellacyanin in glicerol/water and ethylene glycol/water solutions in the temperature range 290–20 K. Biophys Chem 38: 213–224

Cupane A, Leone M, Vitrano E (1993 b) Protein dynamics: conformational disorder, vibrational coupling and anharmonicity in deoxyhemoglobin and myoglobin. Eur Biophys J 21:385–391

Cupane A, Leone M, Vitrano E, Cordone L, Hiltpold UR, Winterhalter KH, Yu W, Di Iorio EE (1993 b) Structure-dynamics-function relationships in Asian Elephant (*Elephas maximus*) myoglobin. An optical spectroscopy and flash-photolysis study on functionally important motions. Biophys J 65:2461–2472

Cusack S, Doster W (1990) Temperature dependence of the low frequency dynamics of myoglobin. Measurement of the vibrational frequency distribution by inelastic neutron scattering. Biophys J 58:243–251

Debrunner PG, Frauenfelder H (1982) Dynamics of proteins. Annu Rev Phys Chem 33:283–299

Dexter DL (1958) Theory of the optical properties of imperfections in non metals. In: Seitz F, Turnbull D (eds) Solid State Physics. Academic Press, New York, pp 353–411

Di Iorio EE, Hiltpold UR, Filipovic D, Winterhalter KH, Gratton E, Vitrano E, Cupane A, Leone M, Cordone L (1991) Protein dynamics: Comparative investigation on heme-proteins with different physiological roles. Biophys J 59:742–754

Di Pace A, Cupane A, Leone M, Vitrano E, Cordone L (1992) Vibrational coupling, spectral broadening mechanisms and anharmonicity effects in carbonmonoxy heme proteins studied by the temperature dependence of the Soret band lineshape. Biophys J 63:475–484

Dooley DM, Rawlings J, Dawson JH, Stephens PJ, Andreasson LE, Malmstrom BG, Gray HB (1979) Spectroscopic studies of rhus vernicifera and polyporus versicolor laccase. Electronic structures of the copper sites. J Am Chem Soc 101:5038–5046

Doster W, Cusack S, Petry W (1989) Dynamical transition of myoglobin revealed by inelastic neutron scattering. Nature 337: 754–756

Eaton WA, Hofrichter J (1981) Polarized absorption and linear dichroism spectroscopy of hemoglobin. Methods Enzymol 76:175–261

Eaton WA, Hanson LK, Stephens PJ, Sutherland JC, Dunn JBR (1978) Optical spectra of oxy- and deoxyhemoglobin. J Am Chem Soc 100:4991–5003

Elber R, Karplus M (1987) Multiple conformational states of proteins: a molecular dynamics analysis of myoglobin. Science 235: 318–321

Frauenfelder H, Parak F, Young RD (1988) Conformational substates in proteins. Annu Rev Biophys Biophys Chem 17:451–479

Gewirth AA, Solomon EI (1988) Electronic structure of plastocyanin: excited state spectral features. J Am Chem Soc 110:3811–3819

Herzberg G (1966) Molecular spectra and molecular structure. III. Van Nostrand Reinhold Company, New York

Huang BK, Rhys A (1950) Theory of light absorption and non-radiative transitions in F-centers. Proc R Soc Ser A 204:406–423

Keller H, Debrunner PG (1980) Evidence for conformational and diffusional mean squares displacements in frozen aqueous solutions of oxyhemoglobin. Phys Rev Lett 45:68–71

Knowles FC, McDonald MJ, Gibson QH (1975) The origin of the Adams-Schuster difference spectrum of oxyhemoglobin. Biochem Biophys Res Commun 66:556–563

Leone M, Cupane A, Vitrano E, Cordone L (1987) Dynamic properties of oxy- and carbonmonoxyhemoglobin probed by optical spectroscopy in the temperature range 300–20 K. Biopolymers 26:1769–1779

Leone M, Cupane A, Vitrano E, Cordone L (1992) Strong vibronic coupling in heme proteins. Biophys Chem 42:111–115

Levy RM, Perahia D, Karplus M (1982) Molecular dynamics of an α-helical polypeptide: temperature dependence and deviation from harmonic behavior. Proc Natl Acad Sci, USA 29:1346–1350

Loncharich RJ, Brooks BR (1990) Temperature dependence of dynamics of hydrated myoglobin. J Mol Biol 215:439–455

Makinen MW, Churg AK (1983) Structural and analytical aspects of the electronic spectra of hemeproteins. In: Lever IABP and Gray HB (eds) Iron porphyrins. Addison-Wesley, Reading Mass, pp 141–235

Markham JJ (1959) Interaction of normal modes with electron traps. Rev Mod Phys 31:956–989

McMillin DR, Morris MC (1981) Further perspectives on the charge transfer transitions of blue copper proteins and the ligand moieties in stellacyanin. Proc Natl Acad Sci, USA 78: 6567–6570

Morikis D, Li P, Bangcharoenpaurpong O, Sage JT, Champion PM (1991) Resonance Raman scattering as a probe of electron-nu-

clear coupling: applications to heme proteins. J Phys Chem 95: 3391–3398

Ormos P, Ansari A, Braunstein D, Cowen BR, Frauenfelder H, Hong MH, Iben IET, Sauke TB, Steinbach P, Young RD (1990) Inhomogeneous broadening in spectral bands of carbonmonoxymyoglobin: the connection between spectral and functional heterogeneity. Biophys J 57:191–199

Parak F, Frolov EN, Mossbauer RL, Goldanskii VI (1981) Dynamics of metmyoglobin crystals investigated by nuclear gamma resonance absorption. J Mol Biol 145:825–833

Parak F, Knapp EW, Kucheida D (1982) Protein dynamics. Mossbauer spectroscopy on deoxymyoglobin crystals. J Mol Biol 161:177–194

Pryce MHL (1966) In: Stevenson RWH (ed) Phonons in perfect lattices and in lattices with point imperfections. Oliver & Boyd, Edinburgh London

San Biagio PL, Vitrano E, Cupane A, Madonia F, Palma MU (1977) Temperature induced difference spectra of oxy and deoxy hemoglobin in the near IR, visible and Soret regions. Biochem Biophys Res Commun 77:1158–1165

Schomacker KT, Champion PM (1986) Investigations of Spectral broadening Mechanisms in Biomolecules: Cytochrome-c. J Chem Phys 84:5314–5325

Schomacker KT, Champion PM (1989) Investigations of the temperature dependence of resonance Raman cross sections: applications to hemeproteins. J Chem Phys 90:5982–5993

Schweitzer-Stenner R, Dannemann U, Dreybrodt W (1992) Investigation of heme distorsions and heme-protein coupling in the isolated subunits of oxygenated human hemoglobin by resonance Raman dispersion spectroscopy. Biochemistry 31:694–702

Schweitzer-Stenner R, Bosenback M, Dreybrodt W (1993) Raman disperiosn spectroscopy probes heme distorsions in deoxy Hb trout IV involved in its T-state Bohr effect. Biophys J 64: 1194–1209

Smith J, Kuczera K, Karplus M (1990) Dynamics of myoglobin: comparison of simulation results with neutron scattering spectra. Proc Natl Acad Sci, USA 87:1601–1605

Solomon EI, Hare JW, Dooley DM, Dawson JH, Stephens PJ, Gray HB (1980) Spectroscopic studies of stellacyanin, plastocyanin and azurin. Electronic structure of the blue copper site. J Am Chem Soc 102:168–178

Srajer V, Champion PM (1991) Investigations of optical line shapes and kinetic hole burning in myoglobin. Biochemistry 30:7390–7402

Srajer V, Schomacker KT, Champion PM (1986) Spectral broadening in biomolecules. Phys Rev Lett 57:1267–1270

Tsubaki M, Srivastava RB, Yu N (1982) Resonance raman investigation of carbon monoxide bonding in (carbonmonoxy) hemoglobin and -myoglobin: detection of Fe–CO stretching and Fe–C–O bending vibrations and influences of the quaternary structure change. Biochemistry 21:1132–1140

Vitrano E, Cupane A, Leone M, Militello V, Cordone L, Salvato B, Beltramini M, Bubacco L, Rocco P (1993) Low temperature optical spectroscopy of cobalt substituted hemocyanin from Carcynus Maenas. Eur Biophys J 22:157–167